Investigation of coated FeCr steels for application as solid oxide fuel cell interconnects under dual-atmosphere conditions

Downloaded from: https://research.chalmers.se, 2026-09-09 12:12 UTC

Citation for the original published paper (version of record):
Reddy, M., Visibile, A., Svensson, J. et al (2023). Investigation of coated FeCr steels for application as solid oxide fuel cell interconnects
under dual-atmosphere conditions. International Journal of Hydrogen Energy, 48(38): 14406-14417.
http://dx.doi.org/10.1016/j.ijhydene.2022.11.278

N.B. When citing this work, cite the original published paper.

research.chalmers.se offers the possibility of retrieving research publications produced at Chalmers University of Technology. It covers all kind of research output: articles, dissertations, conference papers, reports etc. since 2004. research.chalmers.se is administrated and maintained by Chalmers Library

(article starts on next page)

Available online at www.sciencedirect.com

ScienceDirect

journal homepage: www.elsevier.com/locate/he

Investigation of coated FeCr steels for application as solid oxide fuel cell interconnects under dual-atmosphere conditions

Mareddy Jayanth Reddy, Alberto Visibile, Jan-Erik Svensson, Jan Froitzheim[*]

Chalmers University of Technology, Department of Chemistry and Chemical Engineering, Kemivägen 10, 41296 Gothenburg, Sweden

HIGHLIGHTS

- The Ce/Co-coated steels 441, 444 and Crofer 22 APU form a protective oxide scale at 800 °C under dual-atmosphere conditions.
- The Ce/Co-coating eliminates the observed differences in oxide scale thicknesses for the uncoated steels at 800 °C.
- The oxide scales on the fuel side (uncoated) vary in thickness among the selected steels.
- At 600 °C, the coated steels 441 and 444 form non-protective oxides, while the coated Crofer 22 APU remains protective.

GRAPHICAL ABSTRACT

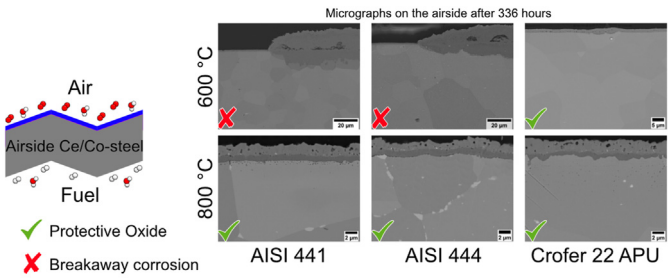

ARTICLE INFO

Article history:
Received 29 September 2022
Received in revised form
22 November 2022
Accepted 24 November 2022
Available online xxx

Keywords:
SOFC
Interconnect

ABSTRACT

Dual-atmosphere conditions are detrimental for the ferritic stainless steel interconnects used in solid oxide fuel cells, resulting in non-protective oxide scale growth on the air side. In this paper, low-cost steels AISI 441 and AISI 444 and the tailor-made Crofer 22 APU, were investigated at 800 °C and 600 °C under dual-atmosphere conditions: air-3%H_2O on one side and Ar-5%H_2-3%H_2O on the other side. At 800 °C, the uncoated and Ce/Co-coated steels formed protective layers of $(Cr,Mn)_3O_4/Cr_2O_3$ and $(Co,Mn)_3O_4/Cr_2O_3$ respectively on the air side after 336 h. However, at 600 °C, the Ce/Co-coated AISI 441 and AISI 444 showed ~20 −25 μm thick $Fe_2O_3/(Fe,Cr)_3O_4$ oxide scale on the air side after 336 h. Ce/Co coated Crofer 22 APU remained protective after 772 h at 600 °C, indicating better resistance to the dual-

* *Corresponding author.*
E-mail address: jan.froitzheim@chalmers.se (J. Froitzheim).

https://doi.org/10.1016/j.ijhydene.2022.11.278

0360-3199/© 2022 The Author(s). Published by Elsevier Ltd on behalf of Hydrogen Energy Publications LLC. This is an open access article under the CC BY license (http://creativecommons.org/licenses/by/4.0/).

Please cite this article as: Reddy MJ et al., Investigation of coated FeCr steels for application as solid oxide fuel cell interconnects under dual-atmosphere conditions, International Journal of Hydrogen Energy, https://doi.org/10.1016/j.ijhydene.2022.11.278

Crofer 22 APU
AISI 441
Hydrogen
Corrosion

atmosphere. The effect of Ce/Co coatings on the air side and the need for coatings on the fuel side are discussed and compared with experimental data.

© 2022 The Author(s). Published by Elsevier Ltd on behalf of Hydrogen Energy Publications LLC. This is an open access article under the CC BY license (http://creativecommons.org/licenses/by/4.0/).

Introduction

To meet the climate goals in line with COP26, environmentally friendly, clean and highly efficient energy conversion devices are needed. Fuel cells and electrolysers are receiving great attention as energy conversion devices. Among the various types of fuel cells, solid oxide fuel cells (SOFC) are high-temperature electrochemical devices that convert the chemical energy of the fuel directly to electrical energy. Moreover, they can be operated in reverse mode as solid oxide electrolyser cells (SOECs), producing hydrogen from electricity and, thereby, supporting the hydrogen economy. SOFCs have attracted considerable interest because of their high efficiency (>70%) [1,2], low emissions, silent operation, and fuel flexibility. A unit cell, comprising an anode, cathode and electrolyte, produces a voltage of approximately 1 V, and several unit cells are connected electrically in series by interconnects, to create stacks with a higher power output. Since an interconnect connects the anode of one cell to the cathode of the next cell, it is exposed to an oxidising atmosphere on one side (usually air) and a reducing atmosphere on the other side (the fuel, usually hydrogen or natural gas).

Recent improvements to the materials and manufacturing techniques used for fuel cell components have lowered the operating temperature of the SOFCs to the range of 600–850 °C, allowing the use of metallic interconnects [3]. Among the different metallic interconnects, chromia-forming ferritic stainless steels (FSS) are most commonly used as interconnects because they have the following characteristics: a thermal expansion coefficient similar to that of the other cell components; a moderately conductive oxide scale; low cost; good formability; ease of manufacturing; and good mechanical properties. However, using chromia-forming FSS results in two major degradation mechanisms in the SOFC: (a) Cr(VI) evaporation, which results in the blocking of the electrochemically active sites on the cathode, thereby preventing the oxygen reduction reaction (also referred to as 'chromium poisoning' [4–6]; and (b) chromia scale growth, resulting in increased electrical resistance across the interconnect. Although chromia scale growth increases the resistance across the cell, it is important that the Cr_2O_3 forms, since it protects the interconnect against rapid oxidation. The rates of chromia scale growth on different alloys are dependent upon the characteristics of the steel, such as composition and microstructure, and the exposure conditions.

The aforementioned degradation mechanisms can be mitigated by the application of protective coatings to the air side of the interconnect [7–12]. In our previous papers [13], we have shown that Cr evaporation decreases about 60-fold and the chromia scale growth diminishes following the application of Ce/Co coatings at 800 °C. The Co layer has a beneficial effect on Cr evaporation. The most effective (in terms of cost and reduced Cr evaporation) thickness of the coating has been found to be 600 nm. In addition, Ce has been found to reduce the oxidation rate of steel. Nevertheless, the studies of the Ce/Co coatings were carried out under single-atmosphere conditions (air). Since the interconnect is exposed to a dual atmosphere (air on one side and fuel, for example, H_2, on the other), it is important to study the interconnect steels and coatings in a dual atmosphere. Yang et al. [14] have shown that the oxide scale formed on the air side of a steel exposed to dual-atmosphere conditions is very different from the oxide scale observed when exposed to air on both sides of the steel. Subsequently, several other researchers have shown the anomalous behaviours of steels when exposed simultaneously to dual atmospheres [14–30]. These anomalous behaviours of the steels are termed 'dual-atmosphere corrosion effect', and they lead either to an increase in the Fe content of the protective scale or to the formation of a non-protective, iron-rich oxide on the air side.

Several authors have reported a dual-atmosphere effect on uncoated steels at 800 °C, although the intensity of the phenomenon varied significantly from one experiment to another. Skilbred et al. [18] have described minor changes to the oxide scale composition without any change to the oxide scale structure. On the other hand, Yang et al. [14] have shown a more severe effect with a significant change in the oxide scale thickness. Such differences might be the result of differences in surface conditions, pre-treatments, and hydrogen concentrations. There is consensus that hydrogen on the fuel side diffuses to the air side and interferes with the oxidation on the air side, although the exact mechanism of this process is highly debated and not yet completely understood. Yang et al. [14] have suggested that hydrogen doping of the chromia scale alters the defect chemistry, resulting in increased metal ion diffusivity; this idea has received support from others [18,25]. Holcomb et al. [16] have suggested that the diffused hydrogen reacts with the inward diffusing oxygen to form water vapour and that this mechanically disrupts the scale. Gunduz et al. [19] have proposed that hydrogen diffusion into the metal causes impaired Cr diffusion along the grain boundaries, resulting in the promotion of an Fe-rich oxide scale.

Yang et al. [31] have demonstrated that increasing the concentration of Cr in the steel results in a less-pronounced dual-atmosphere effect. Moreover, very few studies [32,33] in the literature have compared different steels under dual-atmosphere conditions. To lower the costs, many SOFC manufacturers are considering low-cost commercial steels such as AISI 441, AISI 430 and AISI 444. Thus, it is important to compare the low-cost steels with tailor-made interconnect

Please cite this article as: Reddy MJ et al., Investigation of coated FeCr steels for application as solid oxide fuel cell interconnects under dual-atmosphere conditions, International Journal of Hydrogen Energy, https://doi.org/10.1016/j.ijhydene.2022.11.278

alloys such as Crofer 22 APU under dual-atmosphere conditions. Since it has been established that uncoated steels cannot be used as interconnects because they exhibit high levels of Cr evaporation on the air side, understanding the behaviour of coated steels under dual-atmosphere conditions is highly relevant. Only a few studies have demonstrated the effects of air-side coatings under dual-atmosphere conditions [17,28,29,34]. Since Ce/Co coatings are reported to be extremely effective at reducing Cr evaporation and oxide scale growth, it is important to understand the behaviour of these coating systems under dual-atmosphere conditions.

The dual-atmosphere effect is reported to be most severe at 600 °C than at higher temperatures [19]. Several articles detailing the effects of a dual atmosphere on uncoated steels at 600 °C have been published recently [19,21,22,27,33,35,36]. In general, the air side of an uncoated material at 600 °C is covered with a non-protective, Fe-rich scale due to dual-atmosphere corrosion. However, the effect of coating on the dual-atmosphere effect at this temperature is not discussed in the literature. Since intermediate-temperature SOFCs are operated at this temperature and have gained importance in recent times, it is important to understand the dual-atmosphere effects on coated steels at lower temperatures. Since the Ce/Co coatings have been extensively researched for lower temperatures [37–39], it is of paramount importance to understand the effects of these coatings at lower temperatures.

The aim of this paper was to understand the effects of dual-atmosphere conditions on different steel coating systems. For this reason, two low-cost commercial FSS, AISI 441 and AISI 444 were compared to the tailor-made alloy Crofer 22 APU, both when uncoated and Ce/Co-coated on the air side at 800 °C. Since the dual-atmosphere effects on uncoated steels have been extensively reported at 600 °C, an effort is particularly made on understanding the behaviours of these steels when they were coated on the air side.

Experimental

Samples

Three chromia-forming FSS, AISI 441, AISI 444, and Crofer 22 APU with a thickness of 0.3 mm, were selected for this study. The compositions of these alloys are presented in Table 1. On one surface, a Ce/Co coating with 10 nm of Ce and 600 nm of Co was deposited on the steels using a proprietary Physical Vapour Deposition (PVD) technique at Sandvik Materials Technology AB [40], while the other surface was left in the as-received condition. Circular coupons with a diameter of 21 mm were stamped with a hydraulic press and then ultrasonically cleaned in acetone and ethanol for 10 min each. After the cleaning, the coupons were oxidised in air with a flow rate of 280 ml/min at 800 °C for 20 min by placing the samples in a pre-heated tube furnace. After 20 min, the samples were removed and cooled in laboratory air. This step is similar to stack conditioning, where the stack is heated to ensure the gas tightness of the stack prior to the operation. The conditioning step in the real world is usually long. However, it has previously been shown by Goebel et al. [20,21] that the pre-oxidation time correlates well with the onset of breakaway corrosion. To accelerate the testing, a shorter pre-oxidation step of 20 min was chosen.

Exposures

The samples were placed in a dual-atmosphere sample holder made of 253 MA steel [25,27], with gold rings placed between the sample and the sample holder to make the system gas-tight. In the same exposure, coated and uncoated samples were tested to ensure similar exposure conditions among the different samples. The flow composition was Ar-5% H_2+3% H_2O with a flow rate of 100 sml min^{-1} at the fuel side, while filtered laboratory air+3% H_2O with a flow rate of 8800 sml min^{-1} was used on the air side. This high flow rate on the air side results in a flow regime in which the rate of Cr evaporation is independent of the gas flow [41]. The humid flow was obtained by leading gas through a water bath set at 30 °C. Subsequently, the humid air flow was cooled to 24.4 °C, to obtain an accurate humidity concentration of 3%. A chilled mirror hygrometer (Michell-Optidew Vision) was used to check the humidity level.

The samples were placed in the hottest zone, and complete calibration of the three hot zones of the furnaces was performed, to ensure a homogeneous temperature of ± 5 °C over the entire length of the sample holder. A heating/cooling rate of 1 °C min^{-1} was used for all exposures, to avoid imposing thermal stresses on the oxide scale. Exposures were performed at 600 °C and 800 °C. All exposures were repeated at least once to ensure that the results were reproducible. The exposure time was 2 weeks for all the samples. Some selected samples of Crofer 22 APU were exposed at 600 °C for up to 4 weeks.

Analysis

The surface was analysed using the Zeiss LEO ULTRA 55 FE-SEM scanning electron microscope (SEM). The cross-sections of the coupons were prepared using the Leica EM TIC 3X Broad Ion Beam (BIB) milling system. The resulting cross-sections were analysed using the JEOL 7800F Prime SEM, and the chemical analysis was performed using Energy Dispersive X-ray (EDX) spectroscopy.

Table 1 – Chemical compositions of the selected alloys (in wt.%).

Alloy	Fe	Cr	C	Mn	Si	Ti	Nb	Mo	La
Crofer 22 APU	Bal	22.92	0.004	0.38	0.01	0.06			0.07
AISI 444	Bal	19.03	0.015	0.35	0.40	0.005	0.6	1.86	
AISI 441	Bal	17.56	0.014	0.35	0.59	0.17	0.39		

Please cite this article as: Reddy MJ et al., Investigation of coated FeCr steels for application as solid oxide fuel cell interconnects under dual-atmosphere conditions, International Journal of Hydrogen Energy, https://doi.org/10.1016/j.ijhydene.2022.11.278

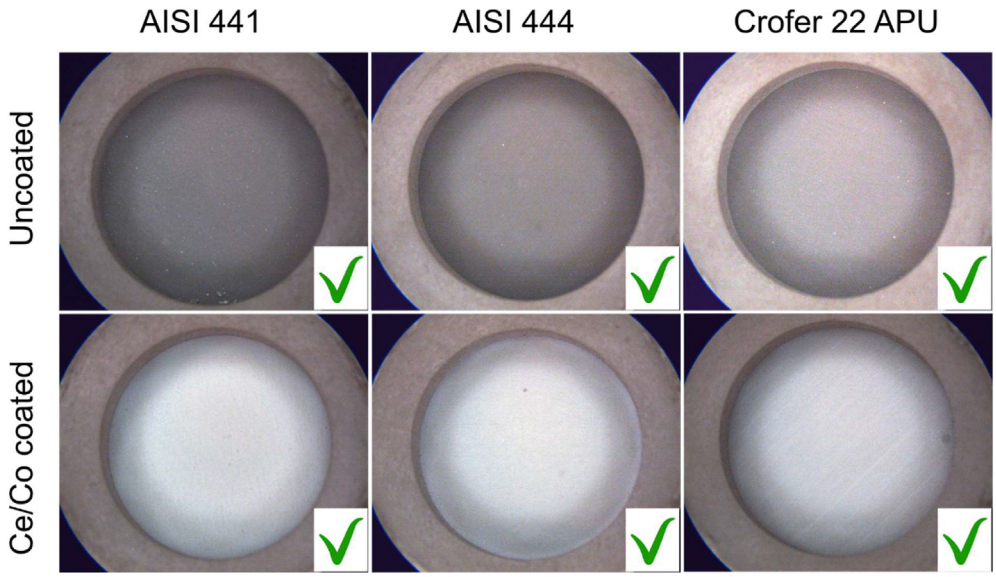

Fig. 1 – Optical micrographs of the air-facing side of the uncoated and the Ce/Co air side coated AISI 441, AISI 444, and Crofer 22 APU, exposed for 336 h in discontinuous dual atmosphere exposure at 800 °C.

Results and discussion

Exposures at 800 °C

Air side

Fig. 1 shows the optical micrographs of the air sides of the uncoated and Ce/Co-coated coupons that were pre-oxidised at 800 °C for 15 min and further exposed to 800 °C for 336 h under dual-atmosphere conditions. All the samples exhibited a protective oxide scale on the air side during the exposure period. The difference in contrast between the uncoated and coated coupons in Fig. 1 is attributed to the different oxide scales formed on these steels, which will be discussed in a later section.

Fig. 2 shows the SEM top views of the air side of the uncoated and Ce/Co-coated coupons exposed at 800 °C for 336 h under dual-atmosphere conditions. The uncoated Crofer 22 APU exhibited a topologically different surface morphology than AISI 441 or AISI 444. Crofer 22 APU showed ridge formation on the oxide scale surface, indicating preferential oxidation at the alloy grain boundaries, while AISI 441 and AISI 444 showed a relatively homogeneous oxide scale. These differences may be attributable to the formation of Laves phases in AISI 441 and AISI 444, which are reported to limit cation diffusion along the grain boundaries. Horita et al. [42]

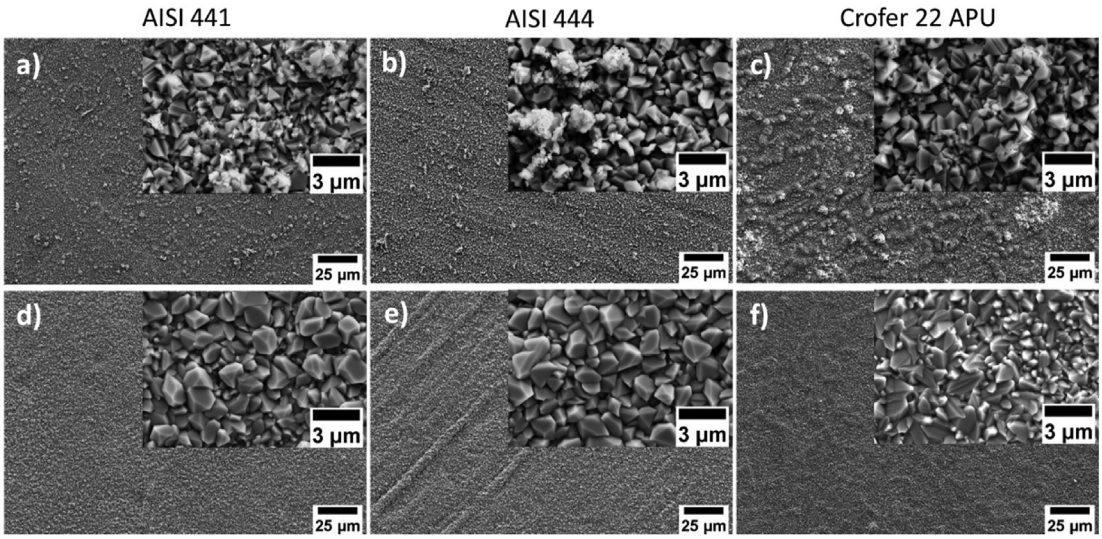

Fig. 2 – SEM micrographs showing the top-view of the air-side of uncoated (a–c) and Ce/Co-coated (d–f) 441, 444 and Crofer 22 APU, respectively, exposed for 336 h in discontinuous dual atmosphere exposure at 800 °C. The inserts in the images show the respective micrographs at higher magnification.

Please cite this article as: Reddy MJ et al., Investigation of coated FeCr steels for application as solid oxide fuel cell interconnects under dual-atmosphere conditions, International Journal of Hydrogen Energy, https://doi.org/10.1016/j.ijhydene.2022.11.278

have shown similar ridge formation on a Laves phase free alloy but found a homogeneous oxide scale on an alloy with Laves phases. The inserts in the images in Fig. 2a–c shows that the surfaces of all the uncoated steels comprise uniform, faceted crystallites of $(Cr,Mn)_3O_4$. On the Ce/Co-coated Crofer 22 APU, ridges at the grain boundaries are less-evident, probably because of the coating. All the coated steel surfaces shown in Fig. 2c–e exhibits a similar morphology. The size of the $(Co,Mn)_3O_4$ crystallites on the coated steels are larger than the $(Cr,Mn)_3O_4$ crystallites on the uncoated steels. The transformation of Co coating to $(Co,Mn)_3O_4$ spinel is widely reported in the literature [17,18,43].

Fig. 3 shows the cross-sections of the air side of the uncoated and Ce/Co-coated coupons exposed to 800 °C for 336 h under dual-atmosphere conditions. The oxide scale thicknesses of the uncoated steels vary slightly. AISI 444 has the thinnest oxide, followed in increasing thickness by Crofer 22 APU and AISI 441. This is similar to the results reported in an earlier study [44]. The oxide scale thickness of the uncoated steels is influenced by the Cr evaporation. It has been reported earlier that Cr evaporation is higher on AISI 444 than from the other steels at 800 °C, which may reflect a thinner oxide scale. That being said, AISI 444 was reported to show lower mass gains than AISI 441 in earlier studies [45,46,58] here the extent of Cr evaporation is similar. In contrast to the uncoated steels, the Ce/Co-coated steels showed similar oxide scale thicknesses after 336 h of exposure.

Laves phase precipitation was observed for AISI 441 and AISI 444. Due to the presence of Mo in AISI 444, the volume of the Laves phases was larger than in AISI 441. Moreover, laves phases in AISI 441 were observed only at the grain boundaries, whereas in AISI 444 they were present at the grain boundaries and also inside the alloy grain. Ti internal oxidation was observed for AISI 441 and Crofer 22 APU in the uncoated and coated forms. The depth of internal oxidation was similar in the coated and the uncoated steels. However, a significant difference was that the patterns of Ti internal oxidation varied significantly between the steels. AISI 441 had Ti internal oxidation only in a region 1 μm deep from the metal-oxide interface. However, Ti internal oxidation in Crofer 22 APU was observed in a region located 10 μm deep from the metal-oxide interface.

Fig. 4 shows the EDX maps of the cross-sections of the air side of the uncoated and Ce/Co-coated AISI 441 coupons exposed to 800 °C for 336 h under dual-atmosphere conditions. The corresponding cross-sections for Crofer 22 APU and AISI 444 show very similar microstructures (supplemental material Figure A1). A more extensive analysis of these materials can be found in Reddy et al. [44]. The oxide scale of the uncoated steel, AISI 441, was composed of two layers: $(Cr,Mn)_3O_4$ spinel on the top and Cr_2O_3 scale beneath, as is commonly found in chromia-forming steels that contain Mn [47]. All the other steels showed a similar oxide scale structure. A previous investigation showed that the chromia scale is nano-grained and that the spinel on the top has larger grains [22]. It has been shown by Niewolak et al. [48] that the formation of spinel on the surface of the metal occurs rapidly, and that complete surface coverage is achieved after 24 h of exposure. The EDX maps of the coated steels showed that the oxide scale is composed of two layers with a $(Co,Mn)_3O_4$ spinel on the top and a Cr_2O_3 scale beneath. The thicknesses of the chromia scales on all the coated steels were similar, at about 1 μm.

Dual atmosphere has been reported to have detrimental effects on ferritic stainless steels exposed at high temperatures in comparison with the same materials exposed to only air. The protectiveness of a chromia scale on the air side can be understood in the context of Wagner's classical theories of internal [49] and selective [50] oxidation. The two important requirements for the formation and maintenance of a chromia scale are that: (i) there is a sufficient activity of the Cr to

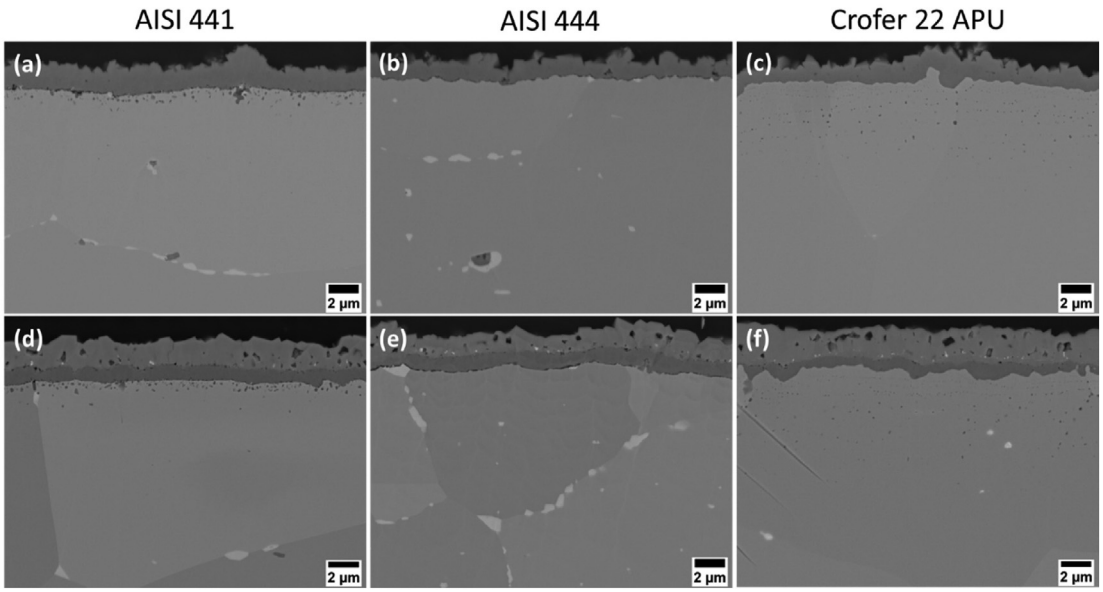

Fig. 3 – SEM micrographs showing the cross-sections of the air side of uncoated (a–c) and Ce/Co-coated (d–f) AISI 441, AISI 444, and Crofer 22 APU, respectively, exposed for 336 h in discontinuous dual atmosphere exposure at 800 °C.

Please cite this article as: Reddy MJ et al., Investigation of coated FeCr steels for application as solid oxide fuel cell interconnects under dual-atmosphere conditions, International Journal of Hydrogen Energy, https://doi.org/10.1016/j.ijhydene.2022.11.278

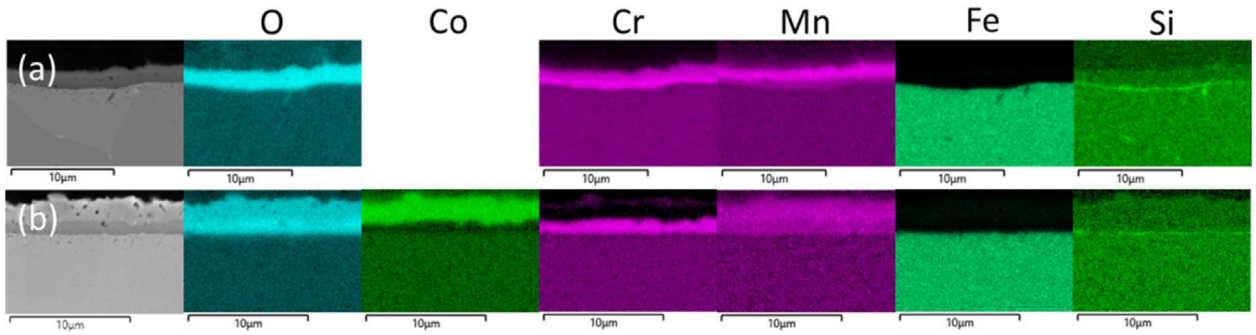

Fig. 4 – SEM micrographs and the corresponding EDX maps of the air side of: (a) uncoated AISI 441; and (b) Ce/Co-coated AISI 441, exposed for 336 h in discontinuous dual atmosphere exposure at 800 °C.

form a scale that covers the entire surface; and (ii) the supply of Cr to the oxide scale is faster than the consumption of Cr at the metal-oxide interface. Gunduz et al. [19] have described the dual-atmosphere effect in great detail using Wagner's classical theories. At 800 °C, the authors further showed that as-received AISI 441 exposed to a dual atmosphere resulted in break-away corrosion while AISI 441 that was peroxidised for 20 min at 800 °C showed no evidence of dual-atmosphere corrosion. Based on that analysis, Gunduz et al. [19] hypothesised that dissolved hydrogen retards grain boundary diffusion of Cr, resulting in the formation of a non-protective, Fe-rich oxide. Nevertheless, in the present study, after 336 h, the uncoated and the Ce/Co-coated coupons showed the formation of a fully protective oxide scale on the air side at 800 °C. Such a protective oxide scale on the uncoated FSS exposed to dual-atmosphere conditions, when pre-oxidised, has been reported by other researchers [19,22]. Moreover, the presence of the coating does not change the protective behaviour of the material since no iron-rich oxide was detected on the air side of any of the coupons.

The consumption of Cr on the air side of the uncoated steel was higher in the presence of water vapour, due to Cr evaporation. Skilbred et al. [17] have shown that the water vapour on the air side influences the oxidation behaviour. Uncoated steels show significant variations in Cr evaporation behaviour in air depending on the alloy composition. However, the Ce/Co-coated steels showed similar Cr evaporation and the rate of Cr evaporation from the coated steels was 60–100 times lower than that from the uncoated steels [44]. Operating the uncoated steels for long periods might result in break-away corrosion due to the combined effect of Cr depletion (due to evaporation) and slower Cr diffusion to the oxide scale due to the presence of hydrogen. Thus, even if the coating is not showing any immediate benefit in the dual atmosphere, it still plays a beneficial role in terms of Cr evaporation, resulting in the prolongation of the sample lifetime.

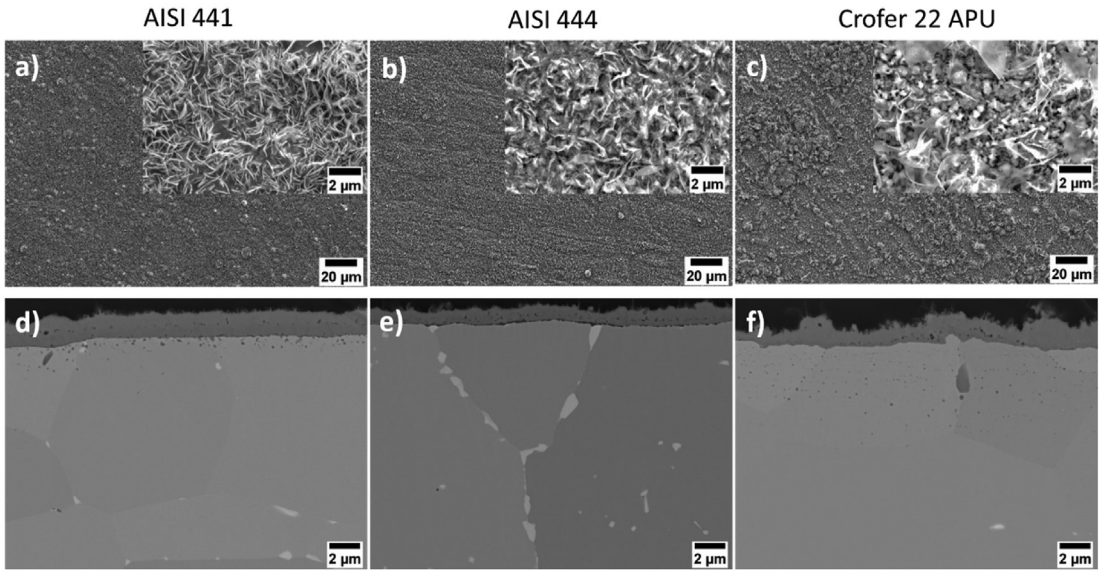

Fig. 5 – SEM micrographs showing the top-view and cross-sectional view of the fuel side of the uncoated: (a,d) AISI 441; (b,e) AISI 444; and (c,f) Crofer 22 APU, respectively, exposed for 336 h in discontinuous dual atmosphere exposure at 800 °C. The inserts in the images show the respective micrographs at higher magnification.

Please cite this article as: Reddy MJ et al., Investigation of coated FeCr steels for application as solid oxide fuel cell interconnects under dual-atmosphere conditions, International Journal of Hydrogen Energy, https://doi.org/10.1016/j.ijhydene.2022.11.278

Fuel side

Fig. 5a–c shows the top view of the fuel side of the uncoated coupons exposed to 800 °C for 336 h under dual-atmosphere conditions. Since the fuel side is not coated, the behaviour, texture, and microstructure at the fuel side of the uncoated and air side Ce/Co-coated coupons are identical. Thus, the top-view and cross-sectional view of the fuel side of the air side Ce/Co-coated coupons are not presented. The top view shows that the oxide scale on the fuel side of all the steels is composed of plate like and needle like structures.

Fig. 5d–f shows cross-sections of the oxide scales, and Fig. 6 shows the EDX maps of the cross-sections of the fuel side of the uncoated coupons exposed to 800 °C for 336 h under dual-atmosphere conditions. Similar to the oxide scale on the uncoated air side, significant differences in oxide scale thickness are observed between the steels. The oxide scale thickness on the fuel side is only slightly thinner than that on the air side of the corresponding uncoated steel. This is in line with observations made by other groups, showing that the oxide scale growth of Mn-containing Fe-Cr alloys in air and H_2/H_2O environment is similar [26,51]. AISI 444 has the thinnest oxide scale, followed by Crofer 22 APU and 441. The oxidation kinetics of the uncoated steels follow similar trends in air and fuel atmospheres. The low oxygen partial pressure (pO_2 ~10^{-18} bar) on the fuel side results in negligible rates of Cr evaporation on the fuel side [52,53]. Since Cr evaporation does not influence the oxide scale thickness, it is concluded that AISI 444 has the lowest oxidation kinetics, followed by Crofer 22 APU and AISI 441 in the fuel atmospheres.

All the oxides in the fuel atmosphere showed a similar structure with two layers, with a $(Cr,Mn)_3O_4$ spinel on the top and a Cr_2O_3 scale at the metal-oxide interface. This observation of a duplex oxide scale in an H_2/H_2O atmosphere agrees with the findings of previous studies on similar Mn-containing FSS [54,55]. A major difference in the oxide scale on the fuel side, as compared to the uncoated air side, is the porosity of the oxide scale. This behaviour has been observed previously [56], usually the porosity is concentrated at the chromia-spinel interface. This might be because of the change in ionic transport in H_2/H_2O compared to air. Ti internal oxidation was observed for AISI 441 and Crofer 22 APU. Similar to the observation made on the air side, the zone of Ti internal oxidation was up to 1 μm deep for AISI 441 and 10 μm for Crofer 22 APU from the oxide scale.

On the steels that were coated with Ce/Co, the Cr-rich scale on the air side (Cr_2O_3) was thinner than the Cr-rich scale on the fuel side [$(Cr,Mn)_3O_4$ and Cr_2O_3]. The thicker Cr-rich oxide scale indicates that the rate of consumption of Cr on the fuel side is higher than on the air side, for the steels when the Ce/Co coating is present. Thus, the corrosion on the fuel side represents a significant degradation mechanism. This is noteworthy because relatively few publications have addressed the degradation mechanisms that occur on the fuel side.

Since there is a trend to move towards using low-cost commercial steels, such as AISI 441 and AISI 444, as interconnects, it is particularly important to study the coatings to reduce the chromia scale growth on the fuel side. The Ce/Co coatings used on the air side are not particularly suitable for use on the fuel side. Skilbred et al. [17] and Sachitanand et al. [56] have reported that Ce/Co coatings on the fuel side lead to the formation of islands of metallic Co. Furthermore, Sachitanand et al. [56] have shown that reactive element (RE) coatings are extremely effective for the fuel side and reduce the k_p value four-fold, as compared to the uncoated steel at 850 °C in fuel atmospheres. Since studies have found no differences in the oxide scales formed on the fuel side between a dual atmosphere and an H_2/H_2O atmosphere [17], RE coatings should be considered for the fuel side. Such coatings might be more effective for use on low-cost steels such as AISI 441 and AISI 444 than for application to Crofer 22 APU, which itself contains REs in the alloy.

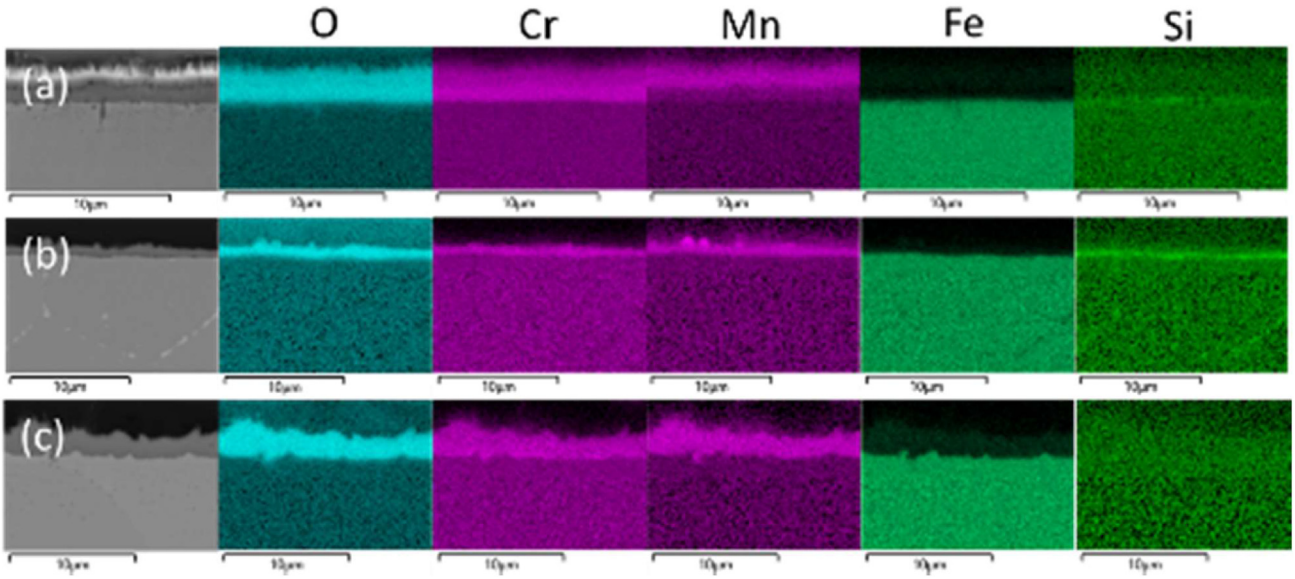

Fig. 6 – SEM micrographs and the corresponding EDX maps of the fuel side of: (a) AISI 441; (b) AISI 444; and (c) Crofer 22 APU exposed for 336 h in discontinuous dual atmosphere exposure at 800 °C.

Please cite this article as: Reddy MJ et al., Investigation of coated FeCr steels for application as solid oxide fuel cell interconnects under dual-atmosphere conditions, International Journal of Hydrogen Energy, https://doi.org/10.1016/j.ijhydene.2022.11.278

Exposure at 600 °C

Fig. 7 shows the optical micrographs of the air side of the Ce/Co-coated coupons pre-oxidised at 800 °C for 20 min in air with 3% H_2O before being exposed to 600 °C for 336 h under dual-atmosphere conditions. The optical images reveal the presence of dark marks on the surface of Ce/Co-coated AISI 441 and AISI 444 after only 168 h of exposure, while such marks are not visible on Crofer 22 APU. After 336 h, the dark spots on Ce/Co-coated AISI 441 and AISI 444 appear to have increased in number and size, while no discernible change is observed on Ce/Co-coated Crofer 22 APU. These spots indicate break-away corrosion due to the dual-atmosphere effect, which results in the formation of iron-rich nodules on the surface. No such spots are observed on Crofer 22 APU even after 772 h of exposure, indicating a protective behaviour of the oxide scale.

Fig. 8a–c shows the SEM micrographs in top-view of the air side, while Fig. 8d–f shows cross-sections of the oxide scales on the air side of the Ce/Co-coated steels exposed at 600 °C for 336 h under dual-atmosphere conditions. The surfaces of the Ce/Co-coated AISI 441 and AISI 444 appear to be similar, in that the surface is partially covered with a non-protective oxide scale, observed as bright islands (50–200 μm in width) and are partially covered with a protective oxide scale. However, the surface of the Ce/Co-coated Crofer 22 APU looks different from the other Ce/Co-coated steels, in that it exhibits an undulating behaviour. The insets in Fig. 8a–c shows that the surface topography of the oxide scale is similar on all the steels for which the oxide scale is protective.

The cross-sections of Ce/Co-coated AISI 441 and AISI 444 shown in Fig. 8d and e, respectively, confirm that the oxide scale comprises both a thin protective region (1 μm) and a thick non-protective region (20 μm). However, on Crofer 22 APU, there are minimal thickness variations (1–2 μm). Fig. 9 shows the EDX maps of the cross-sections of the air side of the Ce/Co-coated AISI 441 and AISI 444 and Crofer 22 APU coupons exposed at 600 °C for 336 h under dual-atmosphere conditions. The oxide scale structure is similar on all the Ce/Co-coated steels in the protective region, with a Co_3O_4 spinel on the top and a Cr_2O_3 scale beneath. Froitzheim et al. [43] have demonstrated that the 600 nm Co coating is oxidised after 30 s at 850 °C. The rate of diffusion of Mn into the Co_3O_4 spinel is much lower at 600 °C than at 800 °C due to slower diffusion kinetics. Thus, only a weak Mn signal is observed in the coatings (see EDX maps in Fig. 9). Falk-Windisch et al. [57] have detected, using STEM/EDX, only 2–3 cation% Mn in the Co spinel after 3300 h at 650 °C.

The oxide scales on the non-protective regions of Ce/Co-coated AISI 441 and AISI 444 are substantially thicker (20–40 μm) than on the protective regions (about 1 μm). These thicker oxide scales are composed of four distinct layers and are observed to have inward-growing and outward-growing parts. On the top is the $(Co,Fe)_3O_4$ spinel. Based on the EDX and TEM analyses carried out by Alnegren et al. [27] and Falk-Windisch et al. [57], the oxide under the $(Co,Fe)_3O_4$ spinel is identified as being Fe-rich. The inward-growing oxide scale is composed of a $(Fe,Cr)_3O_4$ spinel, and the fourth layer is an internal oxidisation zone (IOZ), located at the metal-oxide interface. The inner spinel and the IOZ are formed due to external break-away of the scale, resulting in enhanced inward diffusion of oxygen in that region. Patches of Cr oxide are observed in the IOZ of AISI 441 and AISI 444.

The oxide scale on Ce/Co-coated Crofer 22 APU has both thick and thin regions. The oxide scale in the thinner regions is similar to that observed on Ce/Co-coated AISI 441 and AISI 444 in the protective regions. However, in the thicker regions, the oxide scale on Ce/Co-coated Crofer 22 APU is different in several aspects from the others. First, the oxide scale in the non-protective regions of Ce/Co-coated Crofer 22 APU has a

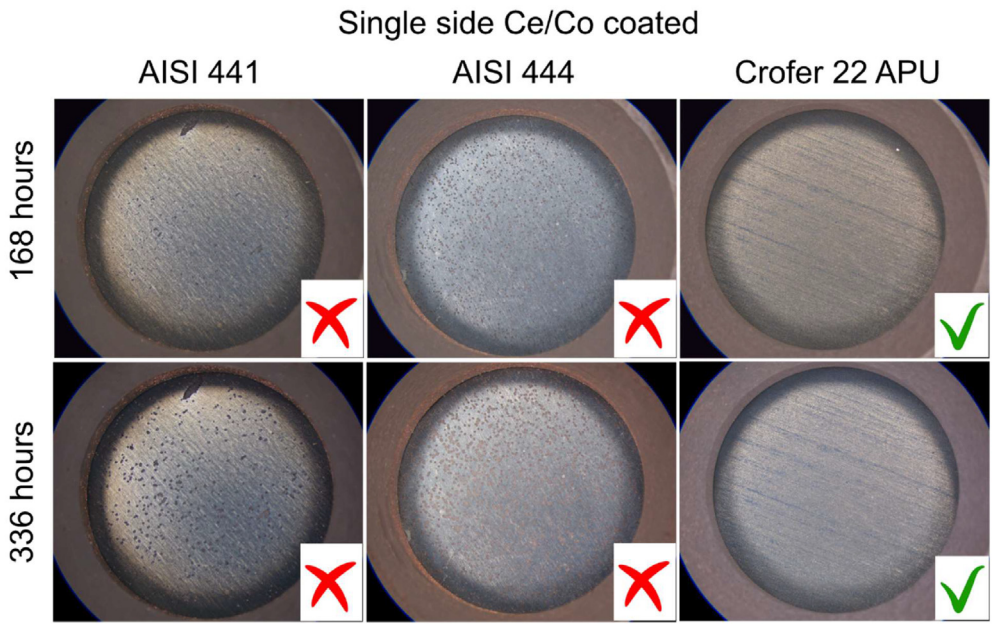

Fig. 7 – Optical micrographs of the air-facing side of Ce/Co air side coated AISI 441, AISI 444, and Crofer 22 APU, after 168 and 336 h in discontinuous dual atmosphere exposure at 600 °C.

Please cite this article as: Reddy MJ et al., Investigation of coated FeCr steels for application as solid oxide fuel cell interconnects under dual-atmosphere conditions, International Journal of Hydrogen Energy, https://doi.org/10.1016/j.ijhydene.2022.11.278

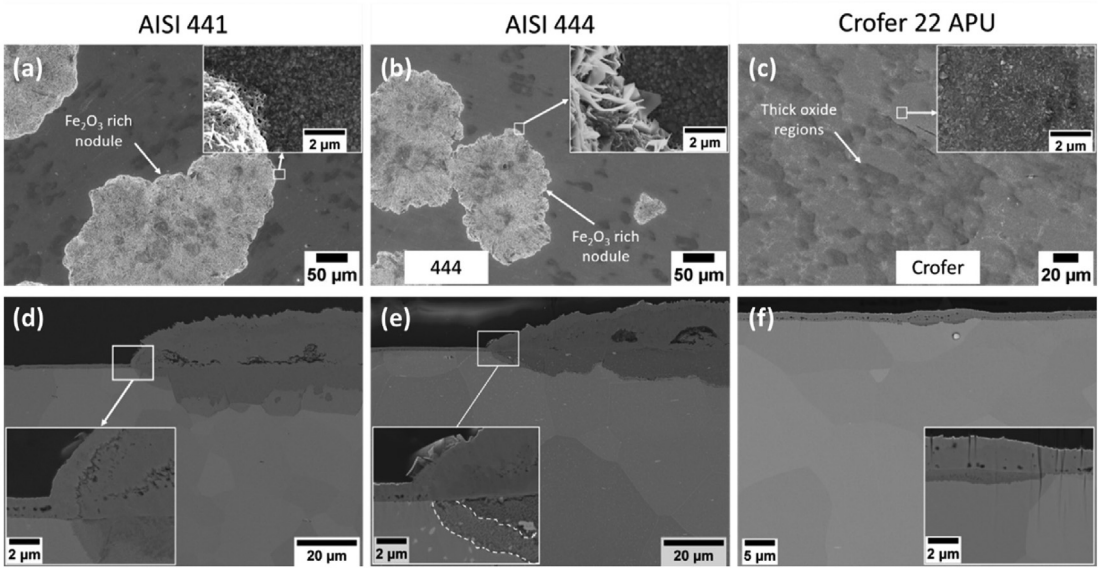

Fig. 8 – SEM micrographs showing the top-view and cross-section view of the air side of Ce/Co-coated (a,d) AISI 441, (b,e) AISI 444 and (c,f) Crofer 22 APU, respectively, exposed for 336 h in discontinuous dual atmosphere exposure at 600 °C. The inserts in the images show the respective micrographs at higher magnification.

thickness of only 3–4 μm, as compared to 20–40 μm thick oxide scales on Ce/Co-coated AISI 441 and AISI 444. The oxide layer on Ce/Co-coated Crofer 22 APU is composed of three layers. The $(Co,Fe)_3O_4$ spinel is on the top, due to coating oxidation. Beneath the $(Co,Fe)_3O_4$ spinel lies an Fe-rich oxide. At the metal-oxide interface, a Cr-rich oxide is found. The undulating behaviour observed in the top-view images (Fig. 8c) is due to the presence of an iron-rich scale underneath the oxidised coating in some regions. From Figs. 8f and 9c, it is unclear as to whether the Ce/Co-coated Crofer 22 APU has started to undergo break-away corrosion or the break-away corrosion has stopped due to the formation of a protective layer under the Fe-rich oxide. Nonetheless, the extent of the phenomenon is much more limited, or at least delayed in time, than in the other two steels, as can be seen from the thicknesses of the non-protective oxides. To explore the ways in which the corrosion progresses, microscopy was performed on the Ce/Co-coated Crofer 22 APU that was exposed for 0 h and 772 h, and the cross-sections are shown in Fig. 10. Already after the pre-oxidation step, an Fe-rich oxide is observed at the metal-oxide interface (Fig. 10a). In contrast, such Fe-rich oxide patches are not evident on AISI 441 or AISI 444 treated in the

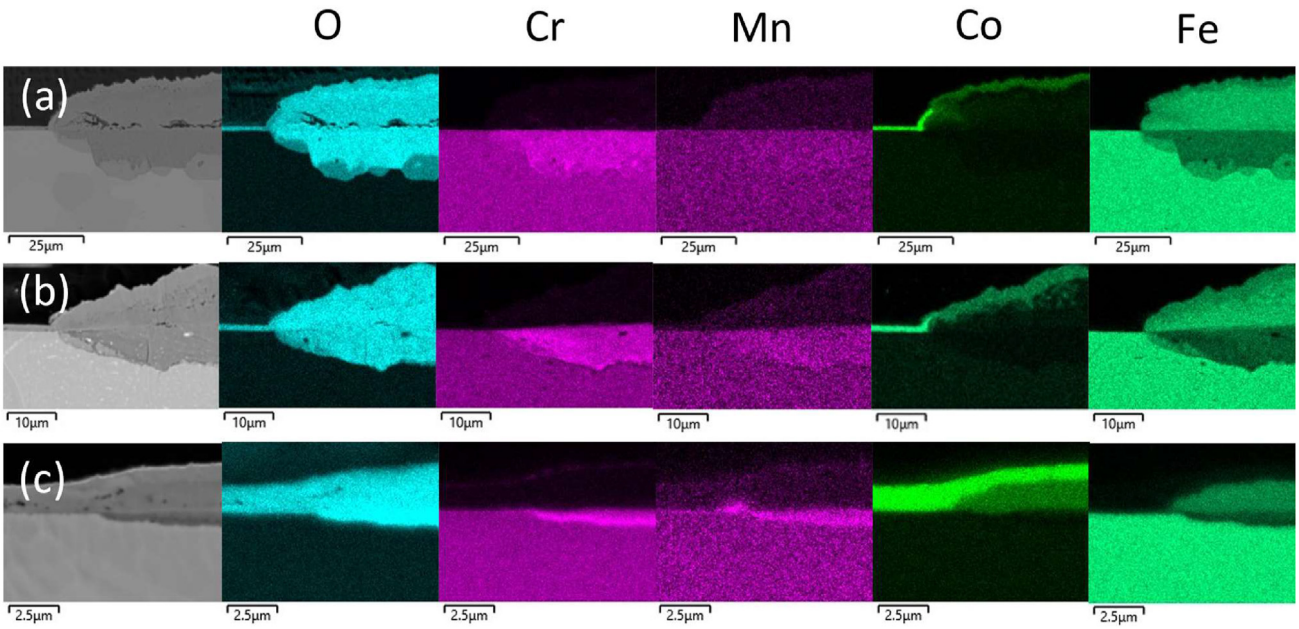

Fig. 9 – SEM micrographs and the corresponding EDX maps of the air side of Ce/Co-coated (a) 441, (b) AISI 444 and (c) Crofer 22 APU, exposed for 336 h in discontinuous dual atmosphere exposure at 600 °C.

Please cite this article as: Reddy MJ et al., Investigation of coated FeCr steels for application as solid oxide fuel cell interconnects under dual-atmosphere conditions, International Journal of Hydrogen Energy, https://doi.org/10.1016/j.ijhydene.2022.11.278

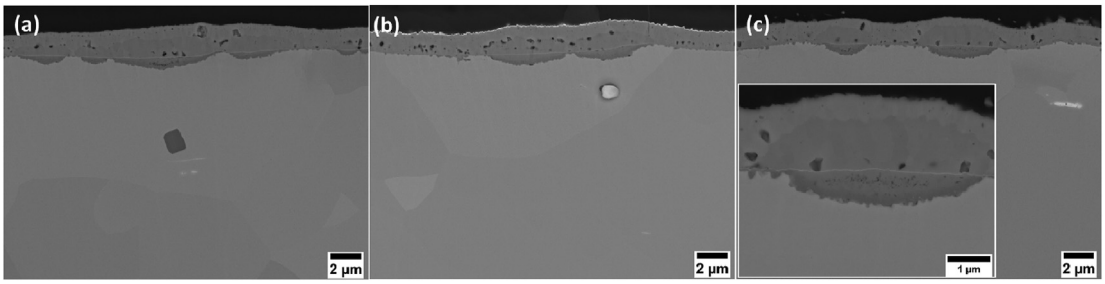

Fig. 10 – SEM micrographs showing the cross-sectional view of the air side of Ce/Co-coated Crofer 22 APU, after discontinuous exposure to a dual atmosphere at 600°Cfor: (a) 0 h (pre-oxidation) (b) 336 h; and (c) 772 h. The inserts in the images show the respective micrographs at higher magnification.

same way. The formation of the Fe-rich oxide after the pre-oxidation step is speculated to be due to the surface finish. After 772 h (Fig. 10c), the oxide scale in the thicker regions is similar to that observed at 0 h and 336 h. Moreover, the oxide scale at the metal-oxide interface appears to be protective and chromia-rich, as shown in the inset of Fig. 10c. This indicates that Ce/Co-coated Crofer 22 APU does not undergo break-away corrosion due to the dual-atmosphere effect, as is the case for Ce/Co-coated AISI 441 or AISI 444.

In the cases of the Ce/Co-coated steels at 600 °C, break-away corrosion is evident on AISI 441 and AISI 444 already after 168 h of exposure. However, such break-away corrosion is not observed on the coated coupons exposed to only air. The observed difference in the oxidation behaviour of the coupons exposed to a single and dual atmosphere is probably due to insufficient diffusion of Cr to the surface, which is related primarily to the presence of hydrogen. This results in the formation of non-protective, Fe-rich oxides on the air side of the steels. However, the dual-atmosphere effect was not observed for Crofer 22 APU even after 772 h because it has a higher Cr content (23 wt%) than either AISI 441 (17 wt%) or AISI 444 (19 wt%). Another reason for the difference could be the presence of Laves phases in AISI 441 and AISI 444, which are known to inhibit the diffusion of Cr and Mn through the grain boundary [42]. Insufficient Cr diffusion towards the surface might then lead to the early formation of iron oxides. Thus, despite the presence of a Ce/Co coating on the air side, the low-cost steels AISI 441 and AISI 444 failed after 168 h, suffering break-away corrosion on the air side, as shown in Fig. 8a and b.

The Ce/Co coatings at the lower temperature of 600 °C behaved slightly different from those at 800 °C. Falk-Windisch et al. [57] have shown that the presence of the reactive element Ce at 650 °C does not influence the oxidisation kinetics of the chromia scale for up to 3300 h. The effect of Ce on chromia scale growth has clearly been observed at higher temperatures, and this phenomenon has been extensively reported at 750 °C [57], 800 °C [44], and 850 °C [45]. However, the presence of Ce in the Ce/Co coating during exposures at lower temperatures results in a lower rate of Fe diffusion into the Co coating [57]. The Ce/Co coating, however, is reported to be very effective in reducing Cr evaporation at 650 °C [39,57]. Cr loss due to evaporation is known to be very important at lower temperatures. Indeed, AISI 441 [58], Crofer 22H [57], and AISI 444 [58] exposed at 650 °C manifested negative mass gains after 500 h because the mass loss due to Cr evaporation was greater than the mass gain due to oxidation. Application of the Ce/Co coating would result in a significantly lower rate of Cr evaporation, which would reduce Cr consumption. Alnegren et al. [22] investigated AISI 441 exposed to dry or to wet (3% H_2O) air under dual-atmosphere conditions, after pre-oxidation for 3 h at 800 °C, and showed that this resulted in break-away corrosion after 1000 h of exposure at 600 °C. These results suggest that other factors, related to hydrogen, are more relevant than Cr evaporation. Nonetheless, the effect of Cr evaporation may still be significant during longer exposures.

Conclusions

This study investigated the effects of airside coatings under dual-atmosphere conditions by exposing 0.3 mm thick uncoated and Ce/Co single-side coated AISI 441, AISI 444 and Crofer 22 APU at 800 °C and 600 °C for 336 h. The uncoated and coated coupons exhibited the formation of a fully protective oxide scale on both the air side and fuel side at 800 °C. The uncoated steels had similar oxidation kinetics on the air side and fuel side at 800 °C. However, the oxidation kinetics of the steels varied slightly. AISI 444 had the lowest oxidation kinetics, followed by Crofer 22 APU and AISI 441. However, the Ce/Co-coated steels had similar oxide scale structures and thicknesses after 336 h. When coated with Ce/Co on the air side, the oxide scale growth was lower than on the fuel side, indicating a need for coating on the fuel side. At 600 °C, the Ce/Co-coated AISI 441 and AISI 444 showed the formation of fast-growing iron-rich oxides in the dual atmosphere. Therefore, a different coating solution needs to be found for the IT-SOFC application. However, Ce/Co-coated Crofer 22 APU did not show the formation of fast-growing, iron-rich oxides, indicating at least a temporary resistance against dual-atmosphere corrosion at 600 °C.

Declaration of competing interest

The authors declare that they have no known competing financial interests or personal relationships that could have appeared to influence the work reported in this paper.

Please cite this article as: Reddy MJ et al., Investigation of coated FeCr steels for application as solid oxide fuel cell interconnects under dual-atmosphere conditions, International Journal of Hydrogen Energy, https://doi.org/10.1016/j.ijhydene.2022.11.278

Acknowledgements

This work was performed within the Swedish High Temperature Corrosion Centre. This project has received funding from the Fuel Cells and Hydrogen 2 Joint Undertaking under Grant Agreement No 826323. This Joint Undertaking receives support from the European Union's Horizon 2020 Research and Innovation programme, Hydrogen Europe and Hydrogen Europe Research. This work was also supported by the strategic innovation program Metalliska Material (Vinnova grant 2021-01003) a joint program of VINNOVA, Formas and the Swedish Energy. This work was performed in part at the Chalmers Material Analysis Laboratory (CMAL).

Appendix A. Supplementary data

Supplementary data to this article can be found online at https://doi.org/10.1016/j.ijhydene.2022.11.278.

REFERENCES

[1] Meng Q, et al. Thermodynamic analysis of combined power generation system based on SOFC/GT and transcritical carbon dioxide cycle. Int J Hydrogen Energy 2017;42:4673–8.
[2] Wang J, Sun X, Jiang Y, Wang J. Assessment of a fuel cell based-hybrid energy system to generate and store electrical energy. Energy Rep 2022;8:2248–61.
[3] Fergus JW. Metallic interconnects for solid oxide fuel cells. Mater Sci Eng, A 2005;397:271–83.
[4] Aphale A, Liang C, Hu B, Singh P. Chapter 6 - cathode degradation from airborne contaminants in solid oxide fuel cells: a review. In: Brandon NP, Ruiz-Trejo E, Boldrin P, editors. Solid oxide fuel cell lifetime and reliability. Academic Press; 2017. p. 101–19. https://doi.org/10.1016/B978-0-08-101102-7.00006-4.
[5] Horita T. Chromium poisoning for prolonged lifetime of electrodes in solid oxide fuel cells - Review. Ceram Int 2021;47:7293–306.
[6] Yokokawa H, et al. Thermodynamic considerations on Cr poisoning in SOFC cathodes. Solid State Ionics 2006;177:3193–8.
[7] Talic B, Venkatachalam V, Hendriksen PV, Kiebach R. Comparison of MnCo2O4 coated Crofer 22 H, 441, 430 as interconnects for intermediate-temperature solid oxide fuel cell stacks. J Alloys Compd 2020;821:153229.
[8] Talic B, Hendriksen PV, Wiik K, Lein HL. Thermal expansion and electrical conductivity of Fe and Cu doped MnCo2O4 spinel. Solid State Ionics 2018;326:90–9.
[9] Yang Z, Xia G, Stevenson JW. Mn1.5Co1.5O4 spinel protection layers on ferritic stainless steels for SOFC interconnect applications. Electrochem Solid State Lett 2005;8.
[10] Zhao Q, Geng S, Gao X, Chen G, Wang F. Ni/NiFe2 dual-layer coating for SOFC steel interconnects application. J. Power Sources Adv. 2020;2:100011.
[11] Zanchi E, et al. Iron doped manganese cobaltite spinel coatings produced by electrophoretic co-deposition on interconnects for solid oxide cells: microstructural and electrical characterization. J Power Sources 2020;455.
[12] Zanchi E, et al. Electrophoretic co-deposition of Fe2O3 and Mn1,5Co1,5O4: processing and oxidation performance of Fe-doped Mn-Co coatings for solid oxide cell interconnects. J Eur Ceram Soc 2019;39:3768–77.
[13] Reddy MJ, Svensson J-E, Froitzheim J. Reevaluating the Cr evaporation characteristics of Ce/Co coatings for interconnect applications. ECS Trans 2021;103:1899–905.
[14] Yang Z, Walker MS, Singh P, Stevenson JW. Anomalous corrosion behavior of stainless steels under SOFC interconnect exposure conditions. Electrochem Solid State Lett 2003;6:B35.
[15] Ardigo MR, et al. Dual atmosphere study of the K41X stainless steel for interconnect application in high temperature water vapour electrolysis. Int J Hydrogen Energy 2015;40:5305–12.
[16] Holcomb GR, Ziomek-Horoz M, Cramer SD, Covino BS, Bullard SJ. Dual-environment effects on the oxidation of metallic interconnects. J Mater Eng Perform 2006;154(15):404–9. 2006.
[17] Skilbred AWB, Haugsrud R. The effect of water vapour on the corrosion of Sandvik sanergy HT under dual atmosphere conditions. Oxid Metals 2013;79:639–54.
[18] Bredvei Skilbred AW, Haugsrud R. The effect of dual atmosphere conditions on the corrosion of Sandvik Sanergy HT. Int J Hydrogen Energy 2012;37:8095–101.
[19] Gunduz KO, et al. The effect of hydrogen on the breakdown of the protective oxide scale in solid oxide fuel cell interconnects. Corrosion Sci 2021;179:109112.
[20] Goebel C, Alnegren P, Faust R, Svensson J-E, Froitzheim J. The effect of pre-oxidation parameters on the corrosion behavior of AISI 441 in dual atmosphere. Int J Hydrogen Energy 2018;43:14665–74.
[21] Goebel C, Alnegren P, Faust RL, Svensson J-E, Froitzheim J. Influence of pre-oxidation on dual atmosphere effect on AISI 441 interconnects for solid oxide fuel cell applications. ECS Trans 2017;78:1559–63.
[22] Alnegren P, Sattari M, Svensson JE, Froitzheim J. Temperature dependence of corrosion of ferritic stainless steel in dual atmosphere at 600–800 °C. J Power Sources 2018;392:129–38.
[23] Yang Z, et al. High temperature oxidation/corrosion behavior of metals and alloys under a hydrogen gradient. Int J Hydrogen Energy 2007;32:3770–7.
[24] Kurokawa H, Kawamura K, Maruyama T. Oxidation behavior of Fe–16Cr alloy interconnect for SOFC under hydrogen potential gradient. Solid State Ionics 2004;168:13–21.
[25] Rufner J, et al. Oxidation behavior of stainless steel 430 and 441 at 800 °C in single (air/air) and dual atmosphere (air/hydrogen) exposures. Int J Hydrogen Energy 2008;33:1392–8.
[26] Stygar M, Brylewski T, Kruk A, Przybylski K. Oxidation properties of ferritic stainless steel in dual Ar–H2–H2O/air atmosphere exposure with regard to SOFC interconnect application. Solid State Ionics 2014;262:449–53.
[27] Alnegren P, Sattari M, Svensson JE, Froitzheim J. Severe dual atmosphere effect at 600 °c for stainless steel 441. J Power Sources 2016;301:170–8.
[28] Leonard ME, Amendola R, Gannon PE, Shong WJ, Liu CK. High-temperature (800 °C) dual atmosphere corrosion of

electroless nickel-plated ferritic stainless steel. Int J Hydrogen Energy 2014;39:15746–53.
[29] Amendola R, et al. Oxidation behavior of coated and preoxidized ferritic steel in single and dual atmosphere exposures at 800°C. Surf Coating Technol 2012;206:2173–80.
[30] Gannon P, Amendola R. High-temperature, dual-atmosphere corrosion of solid-oxide fuel cell interconnects. J Occup Med 2012;64:1470–6.
[31] Yang Z, Walker MS, Singh P, Stevenson JW, Norby T. Oxidation behavior of ferritic stainless steels under SOFC interconnect exposure conditions. J Electrochem Soc 2004;151:B669.
[32] Zhao Y, Fergus JW. Oxidation of alloys 430 and 441 in SOFC dual atmospheres: effects of flow rate and humidity. J Electrochem Soc 2012;159.
[33] Reisert M, et al. Corrosion of chromia-forming and alumina-forming ferritic stainless steels under dual atmosphere exposure conditions. J Electrochem Soc 2021;168:111506.
[34] King MK, Mahapatra MK. Corrosion of nickel and nickel–phosphorous-coated AISI 430 in dry (Ar–3%H2) and humid hydrogen (Ar–3%H2–3%H2O) atmosphere. J Mater Res 2021;36:322–32.
[35] Gagliani L, Visibile A, Gündüz KÖ, Svensson J-E, Froitzheim J. The influence of humidity content on ferritic stainless steels used in solid oxide fuel cell under dual atmosphere conditions at 600°C. ECS Trans 2021;103:1809–15.
[36] Goebel C, Bo C, Svensson J-E, Froitzheim J. The influence of different factors on the dual atmosphere effect observed for AISI 441 interconnects used in solid oxide fuel cells. ECS Trans 2019;91:2261–6.
[37] Falk Windisch H, Svensson J-E, Froitzheim J. Metallic thin-film Co- and Ce/Co-coated steels as interconnect material in IT-SOFC. ECS Trans 2017;78:1607–14.
[38] Goebel C, Asokan V, Khieu S, Svensson JE, Froitzheim J. Self-healing properties of Ce/Co-coated stainless steel under simulated intermediate temperature solid oxide fuel cell conditions. Surf Coating Technol 2021;428:127894.
[39] Tomas M, Goebel C, Svensson J-E, Froitzheim J. Cu-based coatings for IT-SOFC applications. ECS Trans 2019;91:2291–8.
[40] Bernuy-Lopez C, Bexell U, Stenstrom M, Norrby N, Westlinder. J. The time for industrialization has come: a pre-coated solution for the GW scale. ECS Trans 2021;103:1803–8.
[41] Froitzheim J, Ravash H, Larsson E, Johansson LG, Svensson JE. Investigation of chromium volatilization from FeCr interconnects by a denuder technique. J Electrochem Soc 2010;157:B1295.
[42] Horita T, et al. Evaluation of Laves-phase forming Fe–Cr alloy for SOFC interconnects in reducing atmosphere. J Power Sources 2008;176:54–61.
[43] Froitzheim J, et al. Long term study of Cr evaporation and high temperature corrosion behaviour of Co coated ferritic steel for solid oxide fuel cell interconnects. J Power Sources 2012;220:217–27.
[44] Reddy MJ, Chausson TE, Froitzheim J, Svensson J-E. 11-23% Cr steels for solid oxide fuel cell interconnect applications at 800 °C – how the coating determines oxidation kinetics. Int J Hydrog Energy 2023. https://doi.org/10.1016/j.ijhydene.2022.11.326.
[45] Reddy M, Froitzheim J. Report on chemical stability of the coated interconnects. 2020. https://ec.europa.eu/research/participants/documents/downloadPublic?documentIds=080166e5d67d5ca9&appId=PPGMS.
[46] Shu J, Bi H, Li X, Xu Z. The effects of molybdenum addition on high temperature oxidation behavior at 1,000 °c of type 444 ferritic stainless steel. Oxid Metals 2012;78:253–67.
[47] Quadakkers, W. J., Piron-Abellan, J., Shemet, V. & Singheiser, L. Metallic interconnectors for solid oxide fuel cells – a review. 20, 115–127
[48] Niewolak L, Young DJ, Hattendorf H, Singheiser L, Quadakkers WJ. Mechanisms of oxide scale formation on ferritic interconnect steel in simulated low and high pO2 service environments of solid oxide fuel cells. Oxid Metals 2014;82:123–43.
[49] Wagner C. Oxidation of alloys involving noble metals. J Electrochem Soc 1956;103:571.
[50] Wagner C. Reaktionstypen bei der Oxydation von Legierungen. Zeitschrift für Elektrochemie, Berichte der Bunsengesellschaft für Phys. Chemie 1959;63:772–82.
[51] Brylewski T, Nanko M, Maruyama T, Przybylski K. Application of Fe–16Cr ferritic alloy to interconnector for a solid oxide fuel cell. Solid State Ionics 2001;143:131–50.
[52] Opila EJ, et al. Theoretical and experimental investigation of the thermochemistry of CrO 2 (OH) 2 (g). J Phys Chem A 2007;111:1971–80.
[53] Key C, et al. Methods to quantify reactive chromium vaporization from solid oxide fuel cell interconnects. J Electrochem Soc 2014;161:C373–81.
[54] Salgado M de F, Sabioni ACS, Huntz A-M, Rossi ÉH. High temperature oxidation behavior of the AISI 430A and AISI 430E stainless steels in Ar/H2/H2O atmosphere. Mater Res 2008;11:227–32.
[55] Manchili SK. Oxidation behavior of FeCr steels interconnect in low p O2 environments of solid oxide electrolysis cells master of science thesis in materials engineering. 2015.
[56] Sachitanand R, Sattari M, Svensson JE, Froitzheim J. The oxidation of coated SOFC interconnects in fuel side environments. Fuel Cell 2016;16:32–8.
[57] Falk-Windisch H, Claquesin J, Sattari M, Svensson JE, Froitzheim J. Co- and Ce/Co-coated ferritic stainless steel as interconnect material for intermediate temperature solid oxide fuel cells. J Power Sources 2017;343:1–10.
[58] Reddy MJ, Svensson JE, Froitzheim J. Evaluating candidate materials for balance of plant components in SOFC: oxidation and Cr evaporation properties. Corrosion Sci 2021;109671. https://doi.org/10.1016/J.CORSCI.2021.109671.

Please cite this article as: Reddy MJ et al., Investigation of coated FeCr steels for application as solid oxide fuel cell interconnects under dual-atmosphere conditions, International Journal of Hydrogen Energy, https://doi.org/10.1016/j.ijhydene.2022.11.278